Letter

Supercurrent-induced anomalous thermal Hall effect as a new probe to superconducting gap anisotropy

Xiaodong Hu [1], Jung Hoon Han [2], and Ying Ran [1]
[1]*Department of Physics, Boston College, Chestnut Hill, Massachusetts 02467, USA*
[2]*Department of Physics, Sungkyunkwan University, Suwon 16419, Korea*

(Received 29 November 2022; accepted 12 July 2023; published 20 July 2023)

Two-dimensional superconductors have been realized in various atomically thin films such as the twisted bilayer graphene, some of which are anticipated to involve an unconventional pairing mechanism. Due to their low dimensionality, experimental probes of the exact nature of superconductivity in these systems have been limited. We propose, by applying a vertical supercurrent to a bilayer superconductor where the mirror symmetry is naturally broken by the twisting, there will be an anomalous thermal Hall effect induced by the supercurrent that can serve as a sharp probe for the in-plane anisotropy of the superconducting gap function. This effect occurs in the absence of an external magnetic field and spontaneous breaking of the time-reversal symmetry in the ground state. We derive explicit formulas for the induced thermal Hall conductivity and show them to be significant in the examples of twisted cuprates and twisted FeSe where monolayer superconductivity has already been observed. Though technical challenges still exist, we propose this to be a generic probe of the gap anisotropy in a twisted bilayer superconductor.

DOI: 10.1103/PhysRevB.108.L041106

Introduction. The discovery of the correlated insulating phases and superconductivity in twisted bilayer graphene (TBG) [1,2] has spurred intense interest in twisted two-dimensional (2D) heterostructures, leading to the notion of *twistronics* as a new form of electronic device. To understand the (possibly unconventional) superconductivity realized in these systems, intense experimental investigations have been ongoing [3–5]. While the majority of transport studies on twisted bilayers focuses on electrical transport at the moment, thermal transport has long been established as a powerful and complementary tool for investigating the nature of elementary excitations, particularly in superconductors where ordinary electric transport measurement is ineffective [6–11]. More recently, quantized thermal Hall conductivity at low temperature became a signature of the topologically ordered ground states in correlated materials [12,13]. In this Letter, we show that the thermal Hall response can be a sensitive probe of the *gap anisotropy* in twisted bilayer superconductors, or TBSs for short.

The gap function $\Delta_{\boldsymbol{k}}$ of a superconductor has immense implications for the underlying pairing mechanism and the quasiparticle transport. It may be deduced in the angle-resolved photoemission spectroscopy (ARPES) [14–16], or through the quasiparticle interference (QPI) imaging in scanning tunneling spectroscopy [17,18]. Resolving the gap anisotropy in ARPES becomes challenging though for low-temperature superconductors where $\Delta_{\boldsymbol{k}}$ is smaller than the experimental resolution. For twisted heterostructures, resolving the momentum space structure within a small moiré Brillouin zone (BZ) necessitates the QPI imaging over a formidably large area in the real space. As the demand to resolve the gap structure in TBS grows, the limitations of existing experimental probes seem to loom larger. A natural question to ask, at this stage, is whether it is possible to invent a new probe of the gap anisotropy for very small $\Delta_{\boldsymbol{k}}$. Here, we propose a supercurrent-induced anomalous thermal Hall effect (SATHE) as one possible way to directly probe the gap anisotropy in TBS.

Figure 1(a) shows the schematic setup for SATHE. The TBS may be a vertical Josephson junction (JJ) formed by stacking two atomically thin superconducting films with a certain twist angle, or an intrinsic twisted bilayer superconductor as in TBG. SATHE is a nonlinear response of heat, created by simultaneously applying a *vertical* supercurrent $\boldsymbol{J}_S$ and an *in-plane* temperature gradient, with the resulting *transverse in-plane* flow of heat. In contrast to the conventional thermal Hall effect (THE) which occurs when the ground state breaks the time-reversal symmetry (TRS), SATHE can occur for ground states that preserve the TRS. No external magnetic field is required to observe SATHE.

Our proposal thus differs for most proposals of THE including, for instance, Ref. [19] where the JJ spontaneously breaks TRS in the absence of applied supercurrent. It bears a resemblance to the Sodemann-Fu proposal for a nonlinear electrical Hall effect [20,21], in that in both proposals the *unperturbed* ground state preserves TRS. One can think of the nonlinear electrical Hall effect as arising from the first electric field driving an imbalance of the fermion distribution, and the second electric field is used to probe the Hall response. In our proposal, the supercurrent is employed to drive Berry curvature out of its equilibrium form, then a temperature gradient is applied to induce the thermal Hall response. In this sense, SATHE can be taken as a thermal analog of the nonlinear Hall effect.

When the supercurrent is not too large, one can linearize the current-phase relation $\boldsymbol{J}_S \propto \varphi$ and SAHTE becomes the

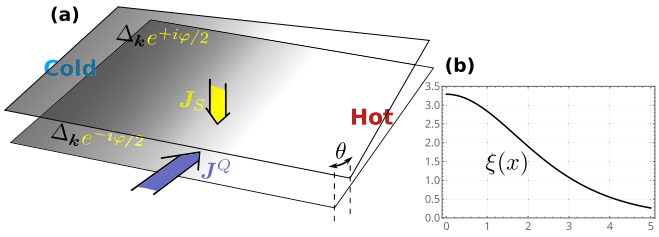

FIG. 1. (a) SATHE for a bilayer superconductor. The vertical supercurrent $\boldsymbol{J}_S$, or equivalently, a pairing phase twist φ between the two layers of, either a vertical JJ or an intrinsic bilayer superconductor, would induce an in-plane thermal Hall effect in a bilayer superconductor. In the former case, an insulating buffer layer may be present (not shown). (b) An illustration for the dimensionless function $\xi(x)$ in Eq. (2).

perturbative change of the thermal Hall conductivity $\delta\kappa_{xy}$ proportional to the phase twist, $\delta\kappa_{xy} \simeq \varphi\chi_{\varphi xy}$, with $\chi_{\varphi xy}$ capturing the nonlinear response of the system. Similar to the nonlinear Hall effect, the breaking of inversion symmetry is necessary to elicit the desired responses. The observation of SATHE additionally requires the breaking of in-plane and out-of-plane mirror symmetries, which are not conditions normally present in the family of nonlinear Hall effects, but are naturally satisfied in the TBS. The conditions for observing SATHE are therefore not any more stringent than those of other proposed nonlinear Hall effects, at least from the perspective of symmetry requirements.

Main results. For TBSs with a multiband electronic structure, the pairing Hamiltonian is generally $\sum_{a,b}\Delta_{\boldsymbol{k}}{}^{a,b}c^\dagger{}_{a,\boldsymbol{k}}c^\dagger{}_{b,-\boldsymbol{k}}$, with a, b ranging over the bands. We first study the simple situation where only the *intraband pairing* is present: $\Delta_{\boldsymbol{k}}{}^{a,b} = 0$ for $a \neq b$. Assuming that $|\Delta_{\boldsymbol{k}}|$ is much smaller than the energy difference between bands in the normal state, we find that a small pairing phase difference φ between the layers in the TBS induces a change of the Berry curvature and leads to the SATHE formula

$$\frac{\delta\kappa_{xy}^{\text{intra}}}{T} = \varphi\frac{\chi_{\varphi xy}^{\text{intra}}}{T} = \varphi\frac{k_B^2}{16\pi^2\hbar}\sum_{\text{FS}}\text{sgn}(v_F) \times\oint_{\text{FS}} dk_\parallel\,\xi\left(\frac{\Delta_{\boldsymbol{k}}(T)}{k_BT}\right)\cdot\partial_{k_\parallel}[\langle u_{\boldsymbol{k}}|\hat{L}|u_{\boldsymbol{k}}\rangle]. \quad (1)$$

Here $\chi_{\varphi xy}^{\text{intra}}$ is the intraband transport coefficient for SATHE, $\xi(x)$ is the dimensionless function [see Fig. 1(b)]

$$\xi(x) \equiv \int_{|x|}^{\infty} dx'\sqrt{x'^2 - x^2}\,\frac{x'}{1+\cosh(x')}, \quad (2)$$

and $|u_{\boldsymbol{k}}\rangle$ is the Bloch state at the Fermi level in the *normal* state. The dimensionless Hermitian operator $\hat{L}$ is the generator of Doppler shift due to φ, and equals $\hat{L} = \text{diag}\{\boldsymbol{1}, -\boldsymbol{1}\}$ in the layer space for a vertical JJ but gets more complicated for an intrinsic bilayer superconductor [see below and Supplemental Material (SM) [22]]. The loop integral is performed over each Fermi surface (FS) and $k_\parallel$ is the counterclockwise tangential momentum at the Fermi surface. The $\text{sgn}(v_F) = \pm 1$ characterizes whether the FS is electronlike or holelike (a single band may host multiple FSs). Clearly if $\Delta_{\boldsymbol{k}}$ is $\boldsymbol{k}$ independent, the loop integral over the FS reduces to a total derivative and vanishes identically.

The $\hat{L}$ operator and Doppler shift. The normal-state tight-binding Hamiltonian for the bilayer can be written in a block form,

$$H_0(\boldsymbol{k}) = \begin{pmatrix} H_0^t(\boldsymbol{k}) & T_\perp(\boldsymbol{k}) \\ T_\perp^\dagger(\boldsymbol{k}) & H_0^b(\boldsymbol{k}) \end{pmatrix}, \quad (3)$$

where t/b labels the top/bottom layer, and $T_\perp$ represents the interlayer hopping. In the superconducting state, pairing terms are introduced. Introducing the pairing phase difference φ due to the applied supercurrent is equivalent to performing a gauge transformation $H_0 \to U(\varphi)H_0U^\dagger(\varphi)$ (Doppler shift) while keeping the pairing terms unchanged, and $\hat{L}$ is its generator: $U(\varphi) \equiv e^{-i\frac{\varphi}{4}\hat{L}}$. For a vertical JJ, $\hat{L} = \text{diag}\{\boldsymbol{1}, -\boldsymbol{1}\}$. For an intrinsic superconductor, $\hat{L}$ depends on the atomic orbital positions normal to the bilayer plane (see SM [22] and also Ref. [23] therein).

For a JJ, since $|u_{\boldsymbol{k}}\rangle$ is the eigenstate of $H_0(\boldsymbol{k})$, $\langle u_{\boldsymbol{k}}|\hat{L}|u_{\boldsymbol{k}}\rangle \in [1, -1]$ serves as the indicator of the layer component of the state. If $T_\perp$ is absent, top/bottom layers decouple and $\langle u_{\boldsymbol{k}}|\hat{L}|u_{\boldsymbol{k}}\rangle = \pm 1$, leading to vanishing SATHE according to Eq. (1), consistent with physical intuitions.

Derivation of Eq. (1). Here, we show how to derive the SATHE formula of Eq. (1) while leaving the more technical parts to SM [22]. The thermal Hall conductance in a 2D superconductor is related to the superconducting Berry curvature [24,25] as

$$\frac{\kappa_{xy}}{T} = -\frac{k_B^2}{2\hbar}\int_{-\infty}^{\infty} dE\,\frac{E^2}{(k_BT)^2}\boldsymbol{\sigma}(E)f'(E), \quad (4)$$

where $f(E)$ is the Fermi-Dirac function, and

$$\boldsymbol{\sigma}(E) \equiv -\sum_{\mathbf{a}}\int_{E_k<E}\frac{d^2k}{(2\pi)^2}\boldsymbol{\Omega}_{\boldsymbol{k}}^{\mathbf{a}}. \quad (5)$$

[Bold fonts are used for quantities related to the superconducting Bogoliubov–de Gennes (BdG) state, to be distinguished from the normal-state ones.] Here, $\boldsymbol{\Omega}_{\boldsymbol{k}}^{\mathbf{a}} = -2\,\text{Im}\langle\partial_{k_x}\mathbf{u}_{\boldsymbol{k}}^{\mathbf{a}}|\partial_{k_y}\mathbf{u}_{\boldsymbol{k}}^{\mathbf{a}}\rangle$ is the superconducting Berry curvature while $\mathbf{a}$ labels bands of the BdG Hamiltonian

$$\mathbf{H}(\boldsymbol{k}) = \begin{pmatrix} H_0(\boldsymbol{k}) & \boldsymbol{\Delta}_{\boldsymbol{k}} \\ \boldsymbol{\Delta}_{\boldsymbol{k}} & -H_0(\boldsymbol{k}) \end{pmatrix}. \quad (6)$$

The BdG Hamiltonian (6) is written in the Nambu basis $\{\psi_{\boldsymbol{k}}, \Lambda^\dagger\psi_{-\boldsymbol{k}}^\dagger\}$ where $\psi_{\boldsymbol{k}}$ is a collection of fermion operators in the band basis, and $\boldsymbol{\Delta}_{\boldsymbol{k}}^\dagger = \boldsymbol{\Delta}_{\boldsymbol{k}}$. The time-reversal transformation works on $\psi_{\boldsymbol{k}}$ as $\psi_{\boldsymbol{k}} \to \Lambda K\psi_{\boldsymbol{k}}$, where K is a complex conjugation and Λ is some unitary operation.

The energy eigenvalues of the BdG Hamiltonian are ordered into pairs $\pm\mathbf{E}_{1,\boldsymbol{k}}, \pm\mathbf{E}_{2,\boldsymbol{k}}, \ldots$ with $\mathbf{E}_{1,\boldsymbol{k}} < \mathbf{E}_{2,\boldsymbol{k}} < \cdots$ and $\mathbf{a} = \pm 1, \pm 2, \ldots$ are used to label the bands such that $\mathbf{E}_{-\mathbf{a},\boldsymbol{k}} = -\mathbf{E}_{\mathbf{a},\boldsymbol{k}}$. Assuming only the intraband pairing is present, we have $\mathbf{E}_{|\mathbf{a}|,\boldsymbol{k}} = (\epsilon_{|\mathbf{a}|,\boldsymbol{k}}^2 + \Delta_{|\mathbf{a}|,\boldsymbol{k}}^2)^{1/2}$, where $\epsilon_{a,\boldsymbol{k}}$ is the normal-state band energy ($a = 1, 2, \ldots$). We assume that only the $a = 1$ band crosses the Fermi level, and all other bands lie strictly above or below it. This allows us to define the interband energy scale as $t \equiv \min|\epsilon_{b,\boldsymbol{k}}|$ ($b \neq 1$). The gap function of the first band is defined as $\Delta_{\boldsymbol{k}} \equiv \Delta_{1,\boldsymbol{k}}$. We will consider the

weak-pairing limit $|\Delta_{\boldsymbol{k}}| \ll t$, so only the lowest-energy states with $\mathbf{a} = \pm 1$ need to be included to the leading-order $\Delta_{\boldsymbol{k}}/t$ expansion of the Berry curvature

$$\boldsymbol{\Omega}^{\mathbf{a}}_{\boldsymbol{k}} \doteq -\,\mathrm{Im}\left\{\frac{\mathrm{Tr}[\mathbf{P_a}\partial_{k_x}\mathbf{H}\mathbf{P}_{-\mathbf{a}}\partial_{k_y}\mathbf{H}\mathbf{P_a}]}{(\mathbf{E_a}-\mathbf{E}_{-\mathbf{a}})^2} - (x \leftrightarrow y)\right\}, \tag{7}$$

where $\mathbf{P_a} \equiv |\mathbf{u}^{\mathbf{a}}_{\boldsymbol{k}}\rangle\langle\mathbf{u}^{\mathbf{a}}_{\boldsymbol{k}}|$ is the projector in the Nambu space.

After a small phase twist φ is turned on, $\mathbf{H}, \mathbf{E}_{\pm\mathbf{a}}, \mathbf{P}_{\pm\mathbf{a}}$ appearing in Eq. (7) all receive some corrections, which propagate through the THE formulas in Eqs. (4) and (5). However, as shown in SM [22], only the change in $\mathbf{P}_{\pm\mathbf{a}}$ is important when the unperturbed ground state obeys TRS. In the end, the intraband pairing contribution gives

$$\delta\boldsymbol{\Omega}^{\mathbf{a},\mathrm{intra}}_{\boldsymbol{k}} \doteq \varphi \sum_{\mathbf{b}\neq\pm\mathbf{a}} 4\,\mathrm{Im}\,\mathrm{Tr}[(\partial_{k_x}\mathbf{P_a})(\partial_{k_y}\mathbf{P}_{-\mathbf{a}})\mathbf{P_b}(\partial_{\varphi}\mathbf{P_a})\mathbf{P_a}] - (x \leftrightarrow y). \tag{8}$$

To the leading order of $\Delta_{\boldsymbol{k}}/t$ expansion and focusing on the $\mathbf{a} = \mathbf{1}$ band, we find

$$\delta\boldsymbol{\Omega}^{\mathbf{1},\mathrm{intra}}_{\boldsymbol{k}} = -\varphi \cdot \frac{\Delta^2_{\boldsymbol{k}}}{4\mathbf{E}^3_{\mathbf{1}}}\left(v_x\partial_{k_y} - v_y\partial_{k_x}\right)\langle u^1_{\boldsymbol{k}}|\hat{L}|u^1_{\boldsymbol{k}}\rangle, \tag{9}$$

with $v_{x,y} \equiv \partial_{k_{x,y}}\epsilon_{1,\boldsymbol{k}}$ the normal-state Fermi velocity.

The change in Berry curvature is now fully described with normal-state wave functions, and exhibits a high concentration near the Fermi surface due to $\mathbf{E}^3_{\mathbf{1}}$ in the denominator. Identifying $\hat{L}|u^1_{\boldsymbol{k}}\rangle = 4i\partial_{\varphi}|u^1_{\boldsymbol{k}}\rangle$, the derivative $\partial_{k_y}\langle u^1_{\boldsymbol{k}}|\hat{L}|u^1_{\boldsymbol{k}}\rangle = 4\Omega_{y,\varphi}$ becomes the *φ-twist Berry curvature*, with one component along the momentum direction and the other along the phase twist φ.

Equation (9) thus demonstrates how the change of Berry curvature in the superconducting state is intricately composed of the gap function, and a mixed Berry curvature in the momentum-phase space. Plugging Eq. (9) into Eq. (4) and after some efforts, the main result of our Letter, Eq. (1), is established.

Interband pairing and nodal superconductivity. When interband pairing is present, the calculation becomes more sophisticated but the final result turns out to be simple. Introducing the normal-state projector $P_c \equiv |u^c_{\boldsymbol{k}}\rangle\langle u^c_{\boldsymbol{k}}|$, the interband pairing gives $\boldsymbol{\Delta}^{\mathrm{inter}}_{\boldsymbol{k}} = \sum_{b\neq c} P_b\boldsymbol{\Delta}_{\boldsymbol{k}}P_c$, which can be eliminated from the BdG Hamiltonian in Eq. (6) by a small unitary rotation

$$e^{i\mathcal{S}\otimes\boldsymbol{\tau}_2}\mathbf{H}(\boldsymbol{k})e^{-i\mathcal{S}\otimes\boldsymbol{\tau}_2} \doteq H_0(\boldsymbol{k})\otimes\boldsymbol{\tau}_3 + \boldsymbol{\Delta}^{\mathrm{intra}}_{\boldsymbol{k}}\otimes\boldsymbol{\tau}_1. \tag{10}$$

Here, $\boldsymbol{\tau}$ are Pauli matrices in the Nambu space, and $\mathcal{S} \equiv \sum_{a\neq b} P_a\boldsymbol{\Delta}_{\boldsymbol{k}}P_b/(\epsilon_{a,\boldsymbol{k}} - \epsilon_{b,\boldsymbol{k}})$ can be viewed small simply because $\boldsymbol{\Delta}_{\boldsymbol{k}}/(\epsilon_{a,\boldsymbol{k}} - \epsilon_{b,\boldsymbol{k}}) \sim \Delta_{\boldsymbol{k}}/t$ is small in the weak-pairing limit. Based on this useful property, all previous perturbative analyses for the intraband pairing can be extended to interband pairing as well, with only one modification replacing the projector $\mathbf{P_a}$ by $\widetilde{\mathbf{P}}_{\mathbf{a}} = e^{-i\mathcal{S}\otimes\boldsymbol{\tau}_2}\mathbf{P_a}e^{i\mathcal{S}\otimes\boldsymbol{\tau}_2}$. Collecting all φ-linear terms contributing to the change of the Berry curvature in Eq. (7) seems to be more complicated, but to the leading order of $\Delta_{\boldsymbol{k}}/t$ the interband contribution can be neatly arranged as [22]

$$\delta\boldsymbol{\Omega}^{\mathbf{1},\mathrm{inter}}_{\boldsymbol{k}} = \varphi \cdot \frac{-\mathbf{d}_{\boldsymbol{k}} \cdot \left(\partial_{k_x}\mathbf{d}_{\boldsymbol{k}} \times \partial_{k_y}\mathbf{d}_{\boldsymbol{k}}\right)}{2\mathbf{E}^3_{\mathbf{1}}}, \tag{11}$$

$$\mathbf{d}_{\boldsymbol{k}} \equiv (\Delta_{\boldsymbol{k}}, G_{\boldsymbol{k}}, \epsilon_{1,\boldsymbol{k}}), \quad G_{\boldsymbol{k}} \equiv \frac{-1}{2}\mathrm{Re}\left[\langle u^1_{\boldsymbol{k}}|\boldsymbol{\Delta}^{\mathrm{inter}}_{\boldsymbol{k}}\hat{L}|u^1_{\boldsymbol{k}}\rangle\right].$$

Equation (11) is clearly reminiscent of the Berry curvature of the effective two-band model

$$\mathbf{H}_{\mathrm{eff}} = \varphi \cdot \partial_{\varphi}\epsilon_{1,\boldsymbol{k}}\boldsymbol{\tau}_0 + \epsilon_{1,\boldsymbol{k}}\boldsymbol{\tau}_3 + \Delta_{\boldsymbol{k}}\boldsymbol{\tau}_1 + \varphi \cdot G_{\boldsymbol{k}}\boldsymbol{\tau}_2. \tag{12}$$

within the perturbative regime. Indeed, we show that $\mathbf{H}_{\mathrm{eff}}$ is exactly the low-energy effective Hamiltonian of the TBS itself with the insertion of a phase twist [22] $\mathbf{H}^{\mathbf{a}}_{\mathrm{eff}} = \widetilde{\mathbf{P}}_{\mathbf{a}}\mathbf{H}[\varphi]\widetilde{\mathbf{P}}_{\mathbf{a}} \doteq \widetilde{\mathbf{P}}_{\mathbf{a}}\mathbf{H}\widetilde{\mathbf{P}}_{\mathbf{a}} + \varphi \cdot \widetilde{\mathbf{P}}_{\mathbf{a}}(\partial_{\varphi}\mathbf{H})\widetilde{\mathbf{P}}_{\mathbf{a}}$, so it could serve as a faithful model to compute $\delta\boldsymbol{\Omega}^{\mathbf{1},\mathrm{inter}}_{\boldsymbol{k}}$.

In calculating $\delta\kappa_{xy}$ in Eq. (4) one should add the two Berry curvature contributions $\delta\boldsymbol{\Omega}^{\mathbf{1}}_{\boldsymbol{k}} = \delta\boldsymbol{\Omega}^{\mathbf{1},\mathrm{intra}}_{\boldsymbol{k}} + \delta\boldsymbol{\Omega}^{\mathbf{1},\mathrm{inter}}_{\boldsymbol{k}}$ in Eq. (5). Among the two, the intraband Berry curvature part can be converted to the Fermi-surface integral form in Eq. (1) but not the interband part. For calculating the latter contribution we can directly use Eqs. (4) and (5) with $\delta\boldsymbol{\Omega}^{\mathbf{1},\mathrm{inter}}_{\boldsymbol{k}}$ given in Eq. (11).

Although in principle the interband contribution for SATHE cannot be neglected, there are many physical situations in which the interband pairing and thus the interband contribution to THE does become small. For instance, if each monolayer of TBS itself is superconducting as in a vertical JJ, $\boldsymbol{\Delta}_{\boldsymbol{k}}$ in Eq. (6) is diagonal in the monolayer band basis. For small twist angle $\theta \ll 1$, a unitary transformation to the band basis also induces interband pairing components in $\boldsymbol{\Delta}_{\boldsymbol{k}}$, which are proportional to θ and can be ignored.

If the system is an intrinsic TBS as TBG, the intra- and interband pairings should be determined self-consistently. For example, for boson-mediated superconductivity, the multiband Eliashberg formulation may be applied, which is characterized by the electron-boson coupling matrix $[\alpha^2(\omega)F(\omega)]_{ab}$, where a, b label bands. Either in the regime where intraband coupling is dominant $[\alpha^2(\omega)F(\omega)]_{a=b} \gg [\alpha^2(\omega)F(\omega)]_{a\neq b}$, or in the regime where the intraband coupling is dominant $[\alpha^2(\omega)F(\omega)]_{a=b} \ll [\alpha^2(\omega)F(\omega)]_{a\neq b}$, it is easy to show that only the intraband pairing is significant [26].

However, there is one particular scenario in which the interband contributions may be dominant, and that is when the superconductivity in the TBS is nodal. In this case, the node would develop a mass gap $m_{\boldsymbol{k}} = \varphi \cdot G_{\boldsymbol{k}}$ right at the nodal point upon the application of a phase twist φ, and a Chern number transfer $\Delta C = \pm\frac{1}{2}$ between the low-energy BdG bands occurs per node. When the net transferred Chern numbers n from all the nodes is nonzero, the system becomes a chiral topological superconductor with quantized THE $\delta\kappa^{\mathrm{inter}}_{xy} \equiv \varphi\chi^{\mathrm{inter}}_{\varphi xy} = ng_0$ in the low-temperature limit $k_BT \ll |m|$, where $\chi^{\mathrm{inter}}_{\varphi xy}$ is the interband transport coefficient for SATHE, and $g_0 \equiv \pi k_B^2T/(6\hbar)$ is the quantum of thermal conductance. In our perturbative treatment, $\chi^{\mathrm{inter}}_{\varphi xy}$ diverges in the low-T regime. This supercurrent-driven topological superconductivity has been discussed in the context of twisted cuprate bilayers [19,27–29] and twisted $NbSe_2$ heterostructures [30].

Applications to FeSe and cuprates. To demonstrate the possibility of observing SATHE in real materials we consider two examples: vertical JJs formed by twisted nodeless FeSe, and the nodal cuprate superconducting films. The $\Delta_{\boldsymbol{k}}$ in both of these 2D superconductors has been well characterized by ARPES due to the large energy scale of $\Delta_{\boldsymbol{k}}$ and high transition temperatures. Note that due to the dimensionless nature of the SATHE response, the supercurrent-induced κ_{xy} only depends on the ratio $\Delta_{\boldsymbol{k}}/k_BT$ as in Eq. (1) and the SATHE response of low-T_c superconductors after appropriate rescaling must be similar to the examples we consider now.

Monolayer FeSe is reported to host a significant nodeless gap anisotropy of the form $\Delta_{\boldsymbol{k}} = \Delta_0 + \Delta_2 \cos 2\theta_{\boldsymbol{k}} + \Delta_4 \cos 4\theta_{\boldsymbol{k}}$, where $\Delta_0 = 9.9$ meV, $\Delta_2 = -1.4$ meV, and $\Delta_4 = 1.2$ meV [16]. The C_4-rotation-related elliptic M pockets positioned at $(\pm\frac{\pi}{2}, \pm\frac{\pi}{2})$ within the two-iron BZ [31–33] can be described by the $\boldsymbol{k}\cdot\boldsymbol{p}$ expansion within Fe's $\{3d_{xz}, 3d_{yz}\}$ orbitals [34,35] as $H_M = [\frac{1}{2m}(k_x^2 + k_y^2) - \mu] + ak_xk_y\tau_z$, where τ_z is a Pauli matrix in the orbital space, $\mu = 0.08$ eV, $1/2m = 1.4$ eV Å^2, and $a = 0.6$ eV Å^2. Since all Fermi pockets are near the zone boundary, the moiré zone folding effect comes into play, and the Bistritzer-MacDonald model [36] is used to construct the normal-state Hamiltonian. For example, to the lowest truncation of the moiré BZ, two hopping processes corresponding to $\delta\boldsymbol{q}^{t,b} = \pm 2K_M \sin\frac{\theta}{2}\hat{k}_y$ are included for all four of the M pockets (see Fig. 2 in SM [22]). We set $T_\perp^{d_{xz}^t - d_{xz}^b}(\delta\boldsymbol{q}^{t,b}) = T_\perp^{d_{yz}^t - d_{yz}^b}(\delta\boldsymbol{q}^{t,b}) \simeq T_\perp = 15$ meV and ignore all interorbital hoppings. After turning on such simple $T_\perp$ with a twist angle $\theta = 11.5^\circ$, the Fermi surfaces reconstruct within the moiré BZ [see Fig. 2(a1)].

Second, we consider a twisted bilayer of cuprates [37] with a d-wave gap anisotropy $\Delta_{\boldsymbol{k}} = \Delta_N \cos 2\theta_{\boldsymbol{k}}$ [38,39] and the reported relation $8.5k_BT_c = 2\Delta_N$ [40,41]. The normal-state bilayer Hamiltonian is constructed by first taking the tight-binding model in Ref. [42] as the monolayer Hamiltonian, and then obtaining the interlayer tunneling $T_\perp(\boldsymbol{k}) = t_z[\frac{1}{4}(\cos k_x^t - \cos k_y^t)(\cos k_y^b - \cos k_y^b) + a_0]$ from the detailed orbital analysis in Refs. [29,43]. The constant $a_0 = 0.4$ is determined from density functional theory (DFT) simulations [43]. We set (i) $t_z = 0.025t_0$ (t_0 = leading hopping strength within the CuO_2 plane) with $\theta = 0.6^\circ$ (chiral topological superconductor) and (ii) $t_z = 0.01t_0$ with $\theta = 17.2^\circ$ (topologically trivial superconductor) and plot the corresponding Fermi surfaces in Figs. 2(b1) and 2(c1), respectively [27,28]. Here, we neglect the moiré zone folding effect for several reasons. First, based on the two-center approximation [36], far away from the zone boundary the moiré zone folding effect may be neglected. Second, the moiré zone folding effect for the Fermi surfaces near the zone boundary does not modify the Fermi-surface topology, leaving the results qualitatively unchanged.

The interband and intraband contributions to SATHE for twisted bilayers of FeSe and cuprates are plotted in Figs. 2(a2)–2(c2). In our linearized scheme, κ_{xy} and $\chi_{\varphi xy}$ are related simply by $\kappa_{xy} = \varphi\chi_{\varphi xy}$. We plot κ_{xy} rather than $\chi_{\varphi xy}$ because the latter apparently diverges as $\varphi \to 0$ while $\kappa_{xy}^{\text{inter}}$ remains finite in a supercurrent-driven topological superconductor as shown in Fig. 2(b2). For illustrative purposes, phase twist $\varphi = 1$ rad is chosen for computation [44]. The interband contribution is evaluated by using the integral formula of Eq. (1). For the interband contribution we rely on Eqs. (4) and (5) with the Berry curvature obtained in Eq. (11).

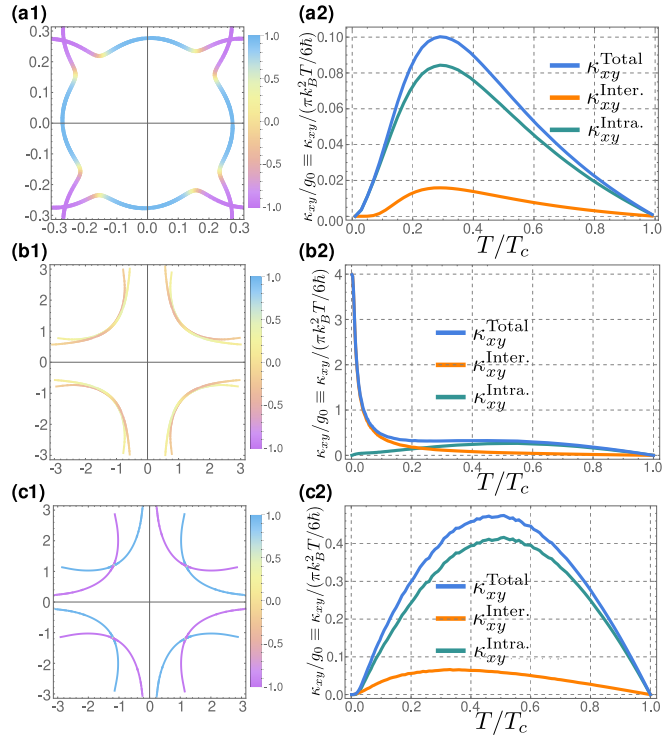

FIG. 2. (a) JJ formed by twisted bilayer FeSe. (b) and (c) The topological nontrivial and trivial phases induced by the supercurrent in JJ formed by twisted bilayer cuprates. The twisted Fermi surfaces are shown in the left panels. For FeSe the moiré zone folding effect plays an important role on the topology of reconstructed Fermi surfaces. The color scheme on each Fermi surface represents the strength of $\langle u_{\boldsymbol{k}}|\hat{L}|u_{\boldsymbol{k}}\rangle \in [-1, 1]$, serving as the indicator of the layer component of states. For all three cases, κ_{xy} is computed in units of the thermal conductance quantum g_0 as a function of temperature, and a simple mean-field temperature dependence of $\Delta_{\boldsymbol{k}}(T) = \Delta_{\boldsymbol{k}}(T=0)\sqrt{1 - T/T_c}$ is implemented. For the topologically nontrivial case (b), gaps ~0.2 meV are generated around superconducting nodes, leading to a Chern number $C = 8$ topological superconductivity, while for the topological trivial case (c) the net Chern number is zero.

As shown in Fig. 2, the intraband contribution plays a dominant role for SATHE in both twisted FeSe [Fig. 2(a2)] and the topological trivial case of twisted cuprates [Fig. 2(c2)], while the interband contribution dominates in the topological nontrivial case of twisted cuprates [Fig. 2(b2)], especially in the low-temperature regime. Note that the κ_{xy} in the proposed SATHE can reach $\sim 10^{-1}$ of the thermal conductance quantum when the gap anisotropy is significant, e.g., in the FeSe example. We conclude that SATHE can be a sizable effect, detectable in the foreseeable future.

Conclusion and discussion. We propose the supercurrent-induced anomalous thermal Hall effect, SATHE, as a new probe to the in-plane gap anisotropy of bilayer superconductors. Different from the conventional thermal Hall effect, the ground state preserves the time-reversal symmetry. A pair of probes—a vertically applied supercurrent and a horizon-

tal temperature gradient—is applied to induce the in-plane nonlinear thermal Hall response. Being a thermal response, it works on 2D superconductors where the usual electrical probes fail. Since no external magnetic field needs to be applied, SATHE avoids the complications of vortices in the mixed state and probes purely the quasiparticle dynamics in superconductors.

Within the BdG framework we showed that SATHE is sensitive to the in-plane gap anisotropy in the twisted bilayer superconductor, and could be large enough to serve as a new experimental probe of gap structure for atomically thin superconducting 2D crystals including twisted bilayer graphene systems, for which experimental probes have been limited due to the low dimensionality. We believe SATHE can eventually find its place as an effective probe of 2D twisted materials, in particular for low T_c superconductors where SATHE can serve as a sensitive measure of the gap anisotropy.

Acknowledgments Y.R. and X.H. acknowledge the support from National Science Foundation under Grant No. DMR-1712128. J.H.H. was supported by the National Research Foundation of Korea (NRF) grant funded by the Korea government (MSIT) (No. 2023R1A2C1002644).

[1] Y. Cao, V. Fatemi, S. Fang, K. Watanabe, T. Taniguchi, E. Kaxiras, and P. Jarillo-Herrero, Unconventional superconductivity in magic-angle graphene superlattices, Nature (London) **556**, 43 (2018).

[2] Y. Cao, V. Fatemi, A. Demir, S. Fang, S. L. Tomarken, J. Y. Luo, J. D. Sanchez-Yamagishi, K. Watanabe, T. Taniguchi, E. Kaxiras *et al.*, Correlated insulator behaviour at half-filling in magic-angle graphene superlattices, Nature (London) **556**, 80 (2018).

[3] M. Oh, K. P. Nuckolls, D. Wong, R. L. Lee, X. Liu, K. Watanabe, T. Taniguchi, and A. Yazdani, Evidence for unconventional superconductivity in twisted bilayer graphene, Nature (London) **600**, 240 (2021).

[4] H. Kim, Y. Choi, C. Lewandowski, A. Thomson, Y. Zhang, R. Polski, K. Watanabe, T. Taniguchi, J. Alicea, and S. Nadj-Perge, Evidence for unconventional superconductivity in twisted trilayer graphene, Nature (London) **606**, 494 (2022).

[5] E. Lake, A. S. Patri, and T. Senthil, Pairing symmetry of twisted bilayer graphene: A phenomenological synthesis, Phys. Rev. B **106**, 104506 (2022).

[6] K. Krishana, N. Ong, Q. Li, G. Gu, and N. Koshizuka, Plateaus observed in the field profile of thermal conductivity in the superconductor $Bi_2Sr_2CaCu_2O_8$, Science **277**, 83 (1997).

[7] M. Chiao, R. W. Hill, C. Lupien, L. Taillefer, P. Lambert, R. Gagnon, and P. Fournier, Low-energy quasiparticles in cuprate superconductors: A quantitative analysis, Phys. Rev. B **62**, 3554 (2000).

[8] M. Sutherland, D. G. Hawthorn, R. W. Hill, F. Ronning, S. Wakimoto, H. Zhang, C. Proust, E. Boaknin, C. Lupien, L. Taillefer, R. Liang, D. A. Bonn, W. N. Hardy, R. Gagnon, N. E. Hussey, T. Kimura, M. Nohara, and H. Takagi, Thermal conductivity across the phase diagram of cuprates: Low-energy quasiparticles and doping dependence of the superconducting gap, Phys. Rev. B **67**, 174520 (2003).

[9] A. C. Durst, A. Vishwanath, and P. A. Lee, Weak-Field Thermal Hall Conductivity in the Mixed State of d-Wave Superconductors, Phys. Rev. Lett. **90**, 187002 (2003).

[10] Y. Zhang, N. P. Ong, P. W. Anderson, D. A. Bonn, R. Liang, and W. N. Hardy, Giant Enhancement of the Thermal Hall Conductivity κ_{xy} in the Superconductor $YBa_2Cu_3O_7$, Phys. Rev. Lett. **86**, 890 (2001).

[11] V. Cvetkovic and O. Vafek, Berry phases and the intrinsic thermal Hall effect in high-temperature cuprate superconductors, Nat. Commun. **6**, 6518 (2015).

[12] M. Banerjee, M. Heiblum, V. Umansky, D. E. Feldman, Y. Oreg, and A. Stern, Observation of half-integer thermal hall conductance, Nature (London) **559**, 205 (2018).

[13] T. Yokoi, S. Ma, Y. Kasahara, S. Kasahara, T. Shibauchi, N. Kurita, H. Tanaka, J. Nasu, Y. Motome, C. Hickey *et al.*, Half-integer quantized anomalous thermal Hall effect in the Kitaev material candidate α-$RuCl_3$, Science **373**, 568 (2021).

[14] Z.-X. Shen, D. S. Dessau, B. O. Wells, D. M. King, W. E. Spicer, A. J. Arko, D. Marshall, L. W. Lombardo, A. Kapitulnik, P. Dickinson, S. Doniach, J. DiCarlo, A. G. Loeser, and C. H. Park, Anomalously large gap anisotropy in the a-b plane of $Bi_2Sr_2CaCu_2O_{8+\delta}$, Phys. Rev. Lett. **70**, 1553 (1993).

[15] H. Ding, M. R. Norman, J. C. Campuzano, M. Randeria, A. F. Bellman, T. Yokoya, T. Takahashi, T. Mochiku, and K. Kadowaki, Angle-resolved photoemission spectroscopy study of the superconducting gap anisotropy in $Bi_2Sr_2CaCu_2O_{8+x}$, Phys. Rev. B **54**, R9678(R) (1996).

[16] Y. Zhang, J. J. Lee, R. G. Moore, W. Li, M. Yi, M. Hashimoto, D. H. Lu, T. P. Devereaux, D.-H. Lee, and Z.-X. Shen, Superconducting Gap Anisotropy in Monolayer FeSe Thin Film, Phys. Rev. Lett. **117**, 117001 (2016).

[17] T. Hanaguri, Y. Kohsaka, J. Davis, C. Lupien, I. Yamada, M. Azuma, M. Takano, K. Ohishi, M. Ono, and H. Takagi, Quasiparticle interference and superconducting gap in $Ca_{2-x}Na_xCuO_2Cl_2$, Nat. Phys. **3**, 865 (2007).

[18] P. O. Sprau, A. Kostin, A. Kreisel, A. E. Böhmer, V. Taufour, P. C. Canfield, S. Mukherjee, P. J. Hirschfeld, B. M. Andersen, and J. S. Davis, Discovery of orbital-selective cooper pairing in FeSe, Science **357**, 75 (2017).

[19] O. Can, T. Tummuru, R. P. Day, I. Elfimov, A. Damascelli, and M. Franz, High-temperature topological superconductivity in twisted double-layer copper oxides, Nat. Phys. **17**, 519 (2021).

[20] I. Sodemann and L. Fu, Quantum Nonlinear Hall Effect Induced by Berry Curvature Dipole in Time-Reversal Invariant Materials, Phys. Rev. Lett. **115**, 216806 (2015).

[21] Q. Ma, S.-Y. Xu, H. Shen, D. MacNeill, V. Fatemi, T.-R. Chang, A. M. Mier Valdivia, S. Wu, Z. Du, C.-H. Hsu *et al.*, Observation of the nonlinear Hall effect under time-reversal-symmetric conditions, Nature (London) **565**, 337 (2019).

[22] See Supplemental Material at http://link.aps.org/supplemental/10.1103/PhysRevB.108.L041106 for detailed derivations on both intraband and interband contributions of SATHE, and a discussion on the nodal origin of the interband contribution and the Fermi-surface reconstruction of twisted bilayer FeSe.

[23] P. J. D. Crowley and L. Fu, Supercurrent-induced resonant optical response, Phys. Rev. B **106**, 214526 (2022).

[24] T. Qin, Q. Niu, and J. Shi, Energy Magnetization and the Thermal Hall Effect, Phys. Rev. Lett. **107**, 236601 (2011).

[25] H. Sumiyoshi and S. Fujimoto, Quantum thermal Hall effect in a time-reversal-symmetry-broken topological superconductor in two dimensions: approach from bulk calculations, J. Phys. Soc. Jpn. **82**, 023602 (2013).

[26] O. V. Dolgov, I. I. Mazin, D. Parker, and A. A. Golubov, Interband superconductivity: Contrasts between Bardeen-Cooper-Schrieffer and Eliashberg theories, Phys. Rev. B **79**, 060502(R) (2009).

[27] P. A. Volkov, J. H. Wilson, K. P. Lucht, and J. H. Pixley, Current- and Field-Induced Topology in Twisted Nodal Superconductors, Phys. Rev. Lett. **130**, 186001 (2023).

[28] P. A. Volkov, J. H. Wilson, K. P. Lucht, and J. H. Pixley, Magic angles and correlations in twisted nodal superconductors, Phys. Rev. B **107**, 174506 (2023).

[29] X.-Y. Song, Y.-H. Zhang, and A. Vishwanath, Doping a moiré Mott insulator: A *t*-*J* model study of twisted cuprates, Phys. Rev. B **105**, L201102 (2022).

[30] X. Hu and Y. Ran, Engineering chiral topological superconductivity in twisted Ising superconductors, Phys. Rev. B **106**, 125136 (2022).

[31] V. Brouet, M. F. Jensen, P.-H. Lin, A. Taleb-Ibrahimi, P. Le Fèvre, F. Bertran, C.-H. Lin, W. Ku, A. Forget, and D. Colson, Impact of the two Fe unit cell on the electronic structure measured by ARPES in iron pnictides, Phys. Rev. B **86**, 075123 (2012).

[32] S. Borisenko, D. Evtushinsky, Z.-H. Liu, I. Morozov, R. Kappenberger, S. Wurmehl, B. Büchner, A. Yaresko, T. Kim, M. Hoesch *et al.*, Direct observation of spin-orbit coupling in iron-based superconductors, Nat. Phys. **12**, 311 (2016).

[33] M. Yi, Z.-K. Liu, Y. Zhang, R. Yu, J.-X. Zhu, J. J. Lee, R. G. Moore, F. T. Schmitt, W. Li, S. C. Riggs *et al.*, Observation of universal strong orbital-dependent correlation effects in iron chalcogenides, Nat. Commun. **6**, 7777 (2015).

[34] D. F. Agterberg, T. Shishidou, J. O'Halloran, P. M. R. Brydon, and M. Weinert, Resilient Nodeless *d*-Wave Superconductivity in Monolayer FeSe, Phys. Rev. Lett. **119**, 267001 (2017).

[35] Y. Ran, F. Wang, H. Zhai, A. Vishwanath, and D.-H. Lee, Nodal spin density wave and band topology of the FeAs-based materials, Phys. Rev. B **79**, 014505 (2009).

[36] R. Bistritzer and A. H. MacDonald, Moiré bands in twisted double-layer graphene, Proc. Natl. Acad. Sci. USA **108**, 12233 (2011).

[37] Note that the currently available cuprate van der Waals materials is Bi2212, which is a bilayer of Cu-O planes. Consequently, a twisted *double* bilayer is more experimental relevant at present. Our twisted bilayer model can viewed as a minimal illustration on SATHE for twisted nodal superconductors.

[38] A. Kanigel, U. Chatterjee, M. Randeria, M. R. Norman, S. Souma, M. Shi, Z. Z. Li, H. Raffy, and J. C. Campuzano, Protected Nodes and the Collapse of Fermi Arcs in High-T_c Cuprate Superconductors, Phys. Rev. Lett. **99**, 157001 (2007).

[39] T. Kondo, W. Malaeb, Y. Ishida, T. Sasagawa, H. Sakamoto, T. Takeuchi, T. Tohyama, and S. Shin, Point nodes persisting far beyond T_c in Bi2212, Nat. Commun. **6**, 7699 (2015).

[40] C. Kendziora, R. J. Kelley, and M. Onellion, Superconducting Gap Anisotropy vs Doping Level in High-T_c Cuprates, Phys. Rev. Lett. **77**, 727 (1996).

[41] H. Anzai, A. Ino, M. Arita, H. Namatame, M. Taniguchi, M. Ishikado, K. Fujita, S. Ishida, and S. Uchida, Relation between the nodal and antinodal gap and critical temperature in superconducting Bi2212, Nat. Commun. **4**, 1815 (2013).

[42] M. Eschrig and M. R. Norman, Effect of the magnetic resonance on the electronic spectra of high-T_c superconductors, Phys. Rev. B **67**, 144503 (2003).

[43] R. S. Markiewicz, S. Sahrakorpi, M. Lindroos, H. Lin, and A. Bansil, One-band tight-binding model parametrization of the high-T_c cuprates including the effect of k_z dispersion, Phys. Rev. B **72**, 054519 (2005).

[44] A Josephson phase twist $\varphi = 1$ rad is taken, primarily to exhibit the strength of the transport coefficient $\chi^{\text{intra}}_{\varphi xy}$ from the intraband contribution along with the quantized behavior of κ_{xy} arising from the interband one. The former component contributes to the thermal Hall conductivity simply as $\kappa^{\text{intra}}_{xy} = \varphi\chi^{\text{intra}}_{\varphi xy}$, as along as we remain within the *linear regime* of the sine current-phase relation, which is satisfied simply because $\sin 1.0 \doteq 0.84 \approx 1.0$. Therefore, the choice $\varphi = 1$ rad can still be considered small in our perturbative treatment, and with such a choice the plot of κ_{xy} also directly reflects the strength of the SATHE transport coefficient $\chi_{\varphi xy}$ that we are concerned with.